Photonic Sensors (2011) Vol. 1, No. 3: 234–250

DOI: 10.1007/s13320-011-0025-4 **Photonic Sensors**

Review

Review on Recent Developments of Fluorescent Oxygen and Carbon Dioxide Optical Fiber Sensors

Cheng-Shane CHU[1], Yu-Lung LO[2], and Ti-Wen SUNG[2]

[1]*Department of Mechanical Engineering, Ming Chi University of Technology, Taishan District, New Taipei City, Taiwan, China*

[2]*Department of Mechanical Engineering, National Cheng Kung University, Tainan, Taiwan, China*

*Corresponding author: Yu-Lung LO E-mail: loyl@mail.ncku.edu.tw

Abstract: Oxygen and carbon dioxide sensors are involved in many chemical and biochemical reactions. Consequently, considerable efforts over years have been devoted to discover and improve suitable techniques for measuring gas concentrations by optical fiber sensors. Optical gas sensors consist of a gas-sensitive dye entrapped in a matrix with a high permeability to gas. With such sensors, gas concentration is evaluated based upon the reduction in luminescence intensity caused by gas quenching of the emitting state. However, the luminescence quenching effect of oxygen is highly sensitive to temperature. Thus, a simple, low-cost plastic optical fiber sensor for dual sensing of temperature and oxygen is presented. Also, a modified Stern-Volmer model is introduced to compensate for the temperature drift while the temperature is obtained by above dual sensor. Recently, we presented highly-sensitive oxygen and dissolved oxygen sensors comprising an optical fiber coated at one end with platinum (II) meso-tetrakis(pentafluorophenyl)porphyrin (PtTFPP) and PtTFPP entrapped core-shell silica nanoparticles embedded in an *n*-octyltriethoxysilane(Octyl-triEOS)/tetraethylorthosilane (TEOS) composite xerogel. Also, two-dimensional gas measurement for the distribution of chemical parameters in non-homogeneous samples is developed and is of interest in medical and biological researches.

Keywords: Oxygen, carbon dioxide, fluorescent dye, optical fiber, temperature effect, modified Stern-Volmer model, core-shell silica nanoparticles

1. Introduction

Major fields of optical fiber technological applications are concerned with humidity, gases and vapors sensing, marine, environmental, medical, chemical and molecular biotechnology analysis, industrial production monitoring, bioprocess control and automotive industry. Oxygen (O_2) is a ubiquitous reactant and an important analyte which must be often quantified in medicine, industry, and environment. Consequently, considerable efforts have been spent over years in developing suitable techniques for the measurement of O_2 concentrations. Fluorescent optical oxygen sensors overcome the limitations of conventional Clark electrode and are widely applied throughout chemical [1], clinical [2] and environmental monitoring [3] fields. Optical oxygen sensors consist of an oxygen-sensitive dye entrapped in a matrix with a high permeability to oxygen. The sensitivity of fluorescent dye depends only on the rate of quenching of the excited states. However, the sensitivity of a fluorescent oxygen

Received: 13 November 2010 / Revised version: 16 February 2011

optical sensor depends on both the quenching rate and the matrix characteristics, e.g. its density, viscosity and hydrophobicity [4]. Therefore, the intrinsic properties of both dye and matrix must be considered when fluorescent oxygen optical sensors are about to be developed.

In general, optimizing the performance of an oxygen sensor requires the use of dyes with long unquenched state lifetime and matrices with high oxygen permeability. Many researchers have reported that sol-gel derived glass is a suitable matrix material for oxygen since it has high oxygen permeability, good mechanical and chemical stability, and superior optical clarity [5]. Furthermore, it has been shown that the use of organically modified silicate (ORMOSIL) matrices improves the response and sensitivity of ruthenium-based oxygen sensors [6, 7]. ORMOSILs can accommodate and disperse analyte-sensitive dyes and have the porous structure, which is an essentially characteristic for improving sensor response.

Carbon dioxide (CO_2) sensing is of fundamental importance in a wide variety of applications to chemical, clinical analysis and environmental monitoring fields. CO_2 in gaseous phase has been measured by infrared (IR) absorptiometry [8]. However, the sensor was both expensive and highly sensitive to the presence of water vapor in gaseous phase. In later studies, optical fiber chemical sensors were proposed as a mean of overcoming the limitations of IR absorptiometry approach [9]. Various optical CO_2 detectors have been proposed over the past decade or so based upon the pH changes induced in an aqueous solution upon exposure to CO_2. Typically, these detectors have the form of either optical-fiber device or planar device, and employ a variety of sensing techniques including fluorescence intensity detection [10, 11], fluorescence resonance energy transfer [12], dual luminophore referencing (DLR) [13], and so on. The pH-sensitive fluorescent dye 1-hydroxy-3,6,8-pyrenetrisulfonic acid trisodium salt (also known as pyranine or HPTS) has distinct absorption/emission bands in visible light region and has been utilized in many aqueous-phase CO_2 optical sensors [14]. In its protonated and deprotonated forms, pyranine exhibits excitation peaks at wavelengths of 396 nm and 460 nm, respectively. The protonated form of pyranine emits in the blue region of the spectrum at a wavelength of 430 nm, whereas the deprotonated form emits in the green region at 515 nm. In typical pyranine-based sensor devices, gaseous CO_2 dissolves in the water contained within a hydrous sensor membrane and forms carbonic acid (H_2CO_3), which subsequently interacts with the deprotonated dye leading to a detectable reduction in the intensity of the green fluorescence [15]. However, the use of polar dyes such as pyranine severely restricts the range of support matrices suitable for immobilization purposes. Specifically, the support material must have good solubility characteristics for the specific polar dye and should retain sufficient moisture to facilitate the water-mediated sensor chemistry. Thus, ORMOSIL matrix is characterized by transparency, photostability and high sensitivity to the external environment and therefore provides a promising solution for a variety of sensing applications. Many researchers have reported that sol-gel derived glass is a suitable matrix material for oxygen or carbon dioxide since it has a high gas permeability, good mechanical and chemical stability, and superior optical clarity. ORMOSILs can accommodate and disperse analyte-sensitive dyes and have the porous structure, which is an essentially characteristic for improving sensor performance.

A working sensor is typically characterized by three basic parameters: sensitivity, selectivity and response time. First, sensitivity is the ability of the sensor to quantitatively measure the test gas under given condition. It is governed by inherent physical and chemical properties of the materials used for matrix. There are a number of concerns: (1) the

materials are transparent, making them highly suitable for quantitative spectrophotometric tests, (2) the materials are chemically inert, photostable and thermally stable, (3) the preparation of the matrix is technically simple, and (4) the matrices of various shapes, as well as thin films, are easily prepared. Hence, the sol-gel process from the above concerns can provide a good matrix with no interaction between fluorescent dye and silica during optical sensing of oxygen and carbon dioxide.

Second, selectivity of a sensor is its ability to sense a particular gas free from interference. The major challenge and drawback of fluorescent optical sensors is their cross-sensitivity. Especially the fluorescence quenching effect of oxygen is highly sensitive to temperature.

Third, response time is a measure of how quickly the maximum signal change is achieved with the change of gas concentration. In addition, reversibility, long term stability, size, and light source power consumption are other factors that could affect the overall performance of the fluorescent optical sensors.

In this brief review, we discuss the sensitivity, the response time, and the temperature effects on fluorescent oxygen sensors. Overall, the results indicate that the dual sensor provides a possible solution for non-contact, simultaneous sensing of temperature and oxygen in general biological and medical applications. Also, a modified Stern-Volmer model is introduced to compensate for temperature drift of oxygen concentration while the temperature is obtained by the dual sensor. In addition, a high-sensitivity fiber-optic carbon dioxide sensor is introduced based on pyranine pH-sensitive fluorescent indicator dye, silica particles, tetraoctylammonium hydroxide (TOAOH) as the phase transfer agent and *n*-octyltriethoxysilane (Octyl-triEOS)/tetraethylorthosilane (TEOS) as the support matrix. Also, the use of hybrid xerogels is intended to improve both the response level and the response speed of CO_2 sensor. The new concept on highly-sensitive oxygen and dissolved oxygen sensors based upon entrapped core-shell silica nanoparticles embedded in a composite xerogel is also introduced.

2. Fluorescent oxygen optical fiber sensors

Optical oxygen sensors consist of an oxygen-sensitive dye entrapped in a matrix with a high permeability to oxygen. The search for optical O_2 sensors to replace conventional electrochemical (Clarke) electrodes is a major goal of current chemical research, with studies focusing on polymers and sol-gel matrices. The advantages offered by traditional commercial electrochemical sensors are well rendered by the comparison between a fiber-optic doped xerogel O_2 sensor and previous electrodes (as illustrated in Table 1). Optical sensors for oxygen are among the most useful sensors known and still experience a substantial amount of research and development. Oxygen by far most often is sensed by virtue of the quenching effect which exerts on certain fluorophores. Optical oxygen sensors consist of an oxygen-sensitive dye entrapped in a matrix with high permeability to oxygen.

Table 1 Advantages of optical O_2 sensors over traditional commercial electrochemical sensors (adapted from oceanoptics.com: http://www.oceanoptics.com/Products/sensorsvselectrodes.htm).

Fiber-optic oxygen sensor systems	Commercial electrodes
Fiber-optic oxygen sensor systems can measure both oxygen gas and dissolved oxygen in gases and liquids	Most electrodes are designed for use in gas or liquids, but not both media
Immune to environmental changes in pH, salinity and ionic strength	Polarographic electrodes can be affected by changes in pH, salinity and ionic strength of the environment
Immune to interference from moisture carbon dioxide, methane and other substances	Electrochemical electrodes are subject to interference from a number of substances and sampling conditions
Long life – more than 1 year	Electrodes have a typical lifetime of just 3 months
Does not consume oxygen, allowing for continuous contact with the sample	Electrodes can consume oxygen of about 0.1 micrograms/hour
Frequent calibration is unnecessary	Calibration may be necessary on an hourly basis
Probe temperature range is –80 ℃ to 80 ℃(up to 110 ℃ for brief periods only)	Temperature range from some electrodes is 0 to 45 ℃

Figure 1 shows a schematic illustration of the experimental arrangement used to characterize the performance of the fluorescent oxygen optical fiber sensor. In the sensing experiments, the fluorescence excitation was provided by a light emitting diode (LED) (LED405E, Thorlabs) with a central wavelength of 405 nm driven by an arbitrary waveform generator (TGA1240, Thurlby Thandar Instruments (TTI) Ltd.) at 10 kHz. The oxygen sensing system consisted of a coated multimode silica glass fiber (1000/1035 μm) and a bifurcated optical fiber (BIF-600-UV-VIS, Ocean Optics). The emission measurements were acquired at a pressure of 101.3 kPa using USB 2000 spectrometer (Ocean Optics).

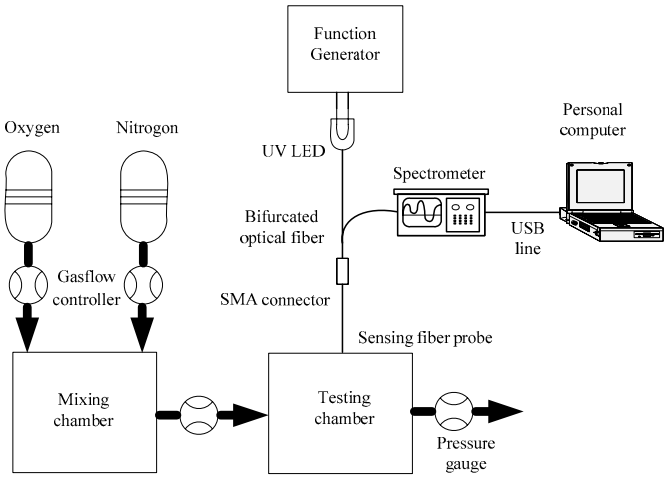

Fig. 1 Schematic diagram of experimental arrangement used for characterization purposes [16].

Luminophore quenching depends on several factors. In the simplest scenario of a luminophore in a homogeneous microenvironment, quenching follows Stern-Volmer equation which is expressed as

$$I_0/I = 1 + K_{sv}[O_2] = 1 + k_q\tau_0[O_2] \quad (1)$$

where I_0 and I represent the steady-state luminescence intensities in the absence and presence of O_2, respectively, K_{sv} is Stern-Volmer quenching constant, $[O_2]$ is O_2 concentration, τ_0 is the excited state luminescence lifetime in the absence of the quencher and k_q is a bimolecular rate constant describing the efficiency of the collisional encounters between the luminophore and the quencher. In the ideal case, a plot of I_0/I against $[O_2]$ has a linear form with a slope equal to K_{sv} and an intercept of unity, allowing a simple single-point sensor calibration.

In 2006, Chu *et al.* [16] reported the high sensitive optical fiber oxygen sensors based on Pt(II) complexes embedded in sol-gel matrix. The ratios I_0/I_{100} as the sensitivity of palladium (II) meso-tetrakis(pentafluorophenyl)porphyrin (PtTFPP) and PtOEP (platinum octaethylporphine) were estimated to be 22 and 48, where I_0 and I_{100} represented the detected fluorescence intensities in pure nitrogen and pure oxygen environments, respectively. Otherwise, the typical Stern-Volmer plot showed a good linearity (as illustrated in Fig. 2). These indicate that PtTFPP and PtOEP immobilized in a sol-gel matrix are photo-stable and highly sensitive to oxygen. In this sensor, the optimal composition of ORMOSIL film is a compromise between adhesion, curing time and sensitivity of the resulting film. The response of the film towards oxygen quenching increases with the organic content of ORMOSIL film due to the improvement in hydrophobicity and oxygen diffusivity.

In 2007, Chu and Lo [17] reported the high performance fiber-optic oxygen sensors based on fluorinated xerogels doped with quenchable Pt(II) complexes. It was shown that the sensitivity of the PtTFPP-doped sensor and the sensitivity of PtOEP-doped sensor were 69 and 83, respectively (as illustrated in Fig. 3), and the response times

ranged from 4 s to 7 s. As a result, the current oxygen sensors exhibited a better sensitive performance, a shorter response time than existing oxygen sensors based on ruthenium dye immobilized in various sol-gel matrices. The main advantages of a Pt(II) dye such as the PtTFPP dye, compared to other Ru(II) complex dyes, are its high luminescence quantum yield, high photo-stability, long lifetime, and larger Stokes shift (100 nm–170 nm) [18]. In this case, the visible absorption of metal porphyrins is attributed to $\pi \rightarrow \pi^*$ transition and large porphyrin ring. The central metal facilitates intersystem crossing to the triplet state, which has a significantly longer τ_0 and enhances oxygen quenching. Pt enhances spin-orbit coupling, so that triple state τ_0 is not so long as to be totally quenched by environmental interactions or trace quenchers [19].

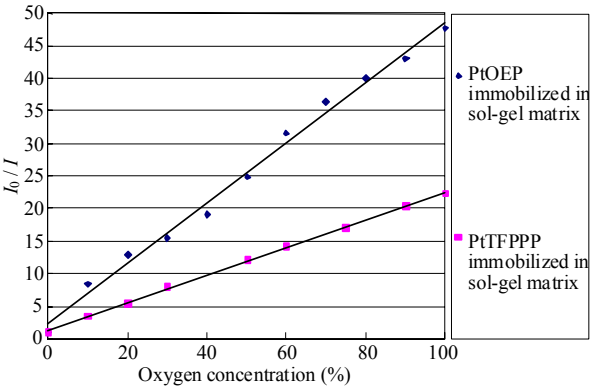

Fig. 2 Stern-Volmer plot for PtTFPP and PtOEP immobilized in a sol-gel matrix and coated on a silica fiber [16].

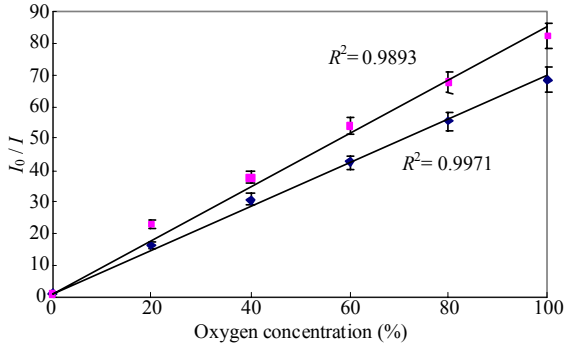

Fig. 3 Stern-Volmer plot for PtTFPP-doped (◆) and PtOEP-doped (■) oxygen sensors [17].

Again, the excellent sensitivity of these sensors is attributed to the uniform distribution of Pt(II) luminophores in the xerogel matrix, and to the improved oxygen diffusivity provided by the fluorinated xerogel. Furthermore, longer excitation and emission wavelengths increase the signal to noise ratio of optical oxygen sensors, which is particularly useful for *in vivo* measurements.

In 2008, Chu and Lo [20] described the highly-sensitive ratiometric fiber-optic oxygen sensors incorporating a sol-gel matrix doped with PtTFPP or PdTFPP metalloporphyrins as oxygen-sensitive material and 7-amino-4-trifluoromethyl coumarin (AFC) as the reference dye. The resulting oxygen sensor was of good linearity in the Stern-volmer plot calibration (Fig. 4). The ratiometric sensing approach presented in this study not only yielded highly sensitivity and reversibility, but also had advantage of suppressing the effects of spurious fluctuations in the intensity of the excitation source and optical transmission properties of the optic fiber.

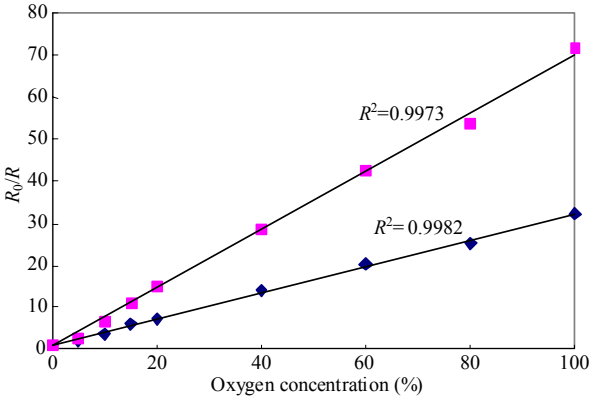

Fig. 4 Stern-Volmer plot of the ratiometric PtTFPP-doped (◆) and PdTFPP-doped (■) oxygen sensors [20].

In the ratiometric fiber optic oxygen sensors, the oxygen concentration is derived from the ratio of the maximum luminescence intensity of PtTFPP or PdTFPP dye to that of oxygen-insensitive AFC dye, i.e.

$$R = I_{\mathrm{Pt(650nm),Pd(670nm)}}/I_{\mathrm{AFC(487nm)}} \quad (2)$$

where $I_{\mathrm{Pt(650nm)}}$ and $I_{\mathrm{Pd(670nm)}}$ represent the steady-state luminescence intensities of the PtTFPP-doped and PdTFPP-doped sensors,

respectively, in the presence of O_2, and $I_{AFC(487nm)}$ is the steady-state luminescence intensity of the reference dye in the presence of O_2. The response of the ratiometric sensors can be evaluated by replacing I_0 and I in the Stern-Volmer equation by R_0 and R, respectively, i.e.

$$R_0/R = 1 + K_{sv}[O_2] = 1 + k_q\tau_0[O_2] \quad (3)$$

where R_0 is the luminescence signal ratio of the sensor in the absence of oxygen.

2.1 Highly sensitive fluorescent sensors based on dye entrapped core-shell particles

Although considerable progress has been made in the optical chemical sensing field in recent years, the development of highly-sensitive detection techniques still remains a major challenge. The sensitivity of sensors which detect the analyte of interest via its interaction with dye molecules embedded in the sensing surface increases with the increase of surface area per unit mass. Accordingly, various designs for chemical sensors with enlarged sensing surfaces have been proposed [21]. However, these sensors invariably involve sophisticated synthesis routes or cumbersome fabrication processes. Silica particles can be synthesized by using a simple process which includes a silica precursor. Diameters in the range of a few nanometers [22] to hundreds of nanometers [23] can be synthesized. Silica particles membranes can have a higher surface area than those of continuous thin films. This large available surface area has the potential to provide unusually high sensitivity in sensing applications. In a recent study, Han *et al.* [24] demonstrated an oxygen sensor based on a phosphorescent dye adsorbed in the pores of mesoporous silica particles deposited with a sub-monolayer coverage on a layer-by-layer self-assembled film. Because of its high surface to volume ratio, a monolayer of micrometer-sized mesoporous silica particles can adsorb sufficient dye to produce a strong photoluminescence (PL) signal while at the same time providing rapid access to oxygen molecules.

The dye entrapped into core-shell silica nanoparticles embedded in the matrix for increasing the surface area per unit mass of the sensing surface plays an important role in the increased sensitivity and linearity. This large available surface area has the potential to provide unusually high sensitivity in sensing applications. In 2010, Chu *et al.* [25] presented a highly-sensitive oxygen sensor that comprised an optical fiber coated at one end with PtTFPP and PtTFPP entrapped core-shell silica nanoparticles embedded in an *n*-octyltriethoxysilane (Octyl-triEOS)/ tetraethylorthosilane (TEOS) composite xerogel. The result reveals that the sensor exhibits a non-linear response at high oxygen concentrations. It can be seen that the oxygen sensor with the PtTFPP-doped dye entrapped core-shell silica particle has sensitivity of 166 (Fig. 5). The quenching process of the optical fiber oxygen sensor at low oxygen concentrations (Fig. 6) can be described by the linear Stern-Volmer equation.

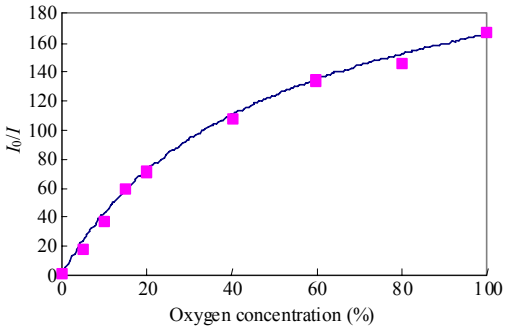

Fig. 5 Stern-Volmer plot of PtTFPP-doped dye entrapped core-shell silica particle oxygen sensor for oxygen concentrations in ranges of 0–100% [25].

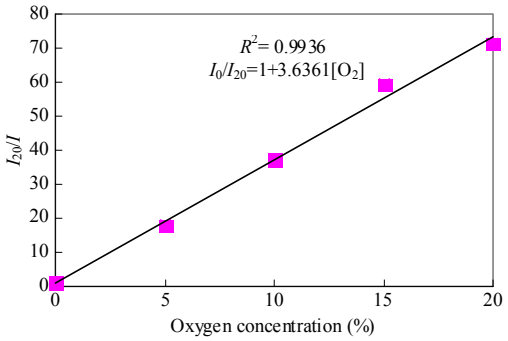

Fig. 6 Stern-Volmer plot of PtTFPP-doped dye entrapped core-shell silica particle oxygen sensor for oxygen concentrations in ranges of 0–20% [25].

Over all, Table 2 compares the performance characteristics of the representative quenchometric O_2 sensors presented in the literature comprising PtTFPP, PtOEP or $Ru(dpp)_3^{2+}$ dyes embedded in various support matrices. Comparing the performance of various sensors, it is apparent that sensors that use a platinum (II) complex as the sensing dye [16, 17, 25] have a significantly higher sensitivity than those using $Ru(dpp)_3^{2+}$ dye [6, 7, 29]. The PtTFPP-doped dye entrapped core-shell silica particle oxygen sensor has higher sensitivity (166), but its response time is slow. The improved sensitivity of oxygen sensor is due to the high surface-to-volume ratio of the dye entrapped core-shell silica nanoparticles embedded in the matrix, which improves the accessibility of oxygen to dye molecules and therefore enhances the quenching effect. Also, the dye entrapped core-shell silica particles play a role in enhancing the sensitivity of the oxygen sensor because of the penetration of substantial amount aerial oxygen molecules through the porous silica shell [25].

Also, the PtTFPP-doped dye entrapped into core-shell silica nanoparticles dissolved oxygen can be designed. Figures 7(a) and 7(b) present the room-temperature fluorescence spectra of the PtTFPP-doped dissolved oxygen sensor under dissolved oxygen concentrations ranging from 0–40 mg/L and 4.4 mg/L–40 mg/L, respectively. Note that in acquiring the relative fluorescence intensity data, the integration time of charge coupled device (CCD) spectrometer was set at 30 ms, and as a result, the sensor exhibited a strong fluorescent response at 650 nm. The distilled water containing different concentrations of dissolved oxygen were obtained by bubbling pure oxygen and nitrogen slowly through distilled water at room temperature for at least 15 min. The dissolved oxygen concentrations up to 40 mg/L were checked with a calibrated dissolved oxygen meter (Oxi 3210, WTW).

Table 2 Comparison of performance characteristics of the oxygen sensors.

Oxygen-sensitive dye	Support matrix	Response time	I_{N_2} / I_{O_2}	Ref.
PtTFPP	fluoropolymer	N_2 to O_2 : 5.6 s O_2 to N_2 : 32 s	15.4	[26]
PtTFPP	Polystyrene polymer	N_2 toO_2 : 18 s O_2 to N_2 : 60 s	3	[27]
PtTFPP	MTEOS	Not available	28	[28]
PtTFPP	Octyl-triEOS/ TEOS	0 O_2 to100% O_2 : 0.6 s 100% O_2 to 0 O_2 : 5 s	22	[16]
PtTFPP	*n*-propyl-TriMOS/ TFP-TriMOS	0 O_2 to100% O_2 : 3.7 s 100% O_2 to 0 O_2 : 5.3 s	68.7	[17]
PtTFPP and dye entrapped core-shell nanoparticles	Octyl-triEOS/ TEOS	0 O_2 to100% O_2 : 1.3 s 100% O_2 to 0 O_2 : 18.6 s	166	[25]
PtTFPP and silica nanoparticles	Octyl-triEOS/ TEOS	0 O_2 to100% O_2 : 6.8 s 100% O_2 to 0 O_2 : 41.4 s	106	[25]
$Ru(dpp)_3^{2+}$	TEOS	0 O_2 to100% O_2 : 3.5 s 100% O_2 to 0 O_2 : 30 s	12	[29]
$Ru(dpp)_3^{2+}$	Octyl-triEOS/ TEOS	Not available	16.5	[6]
$Ru(dpp)_3^{2+}$	*n*-propyl-TriMOS/ TFP-TriMOS	Sensors response times were less than 5 s	35	[7]

PtTFPP: platinum tetrakis pentrafluoropheny porphine

$Ru(dpp)_3^{2+}$: Ru(II)-tris(4,7-diphenyl-1,10-phenanthroline) chloride

MTEOS: methyltriethoxysilane

TEOS: tetraethoxysilane

Octyl-triEOS: *n*-octyltriethoxysilane

n-propyl-TriMOS: *n*-propyltrimethoxysilane

TFP-TriMOS: 3,3,3-trifluoropropyltrimethoxysliane

I_{N_2} : the fluorescence intensities in the absence of oxygen

I_{O_2} : the fluorescence intensities in the 100% oxygen

Figure 8 shows the variation of I_0/I with dissolved oxygen concentrations for the optical fiber dissolved oxygen sensor. It can be seen that the optical fiber dissolved oxygen sensor has overall sensitivity of 117 in the range of 0–40 mg/L. The I_0/I values of the PtTFPP-doped dissolved sensor at dissolved oxygen concentrations of 0, 4.4 mg/L, 8.6 mg/L, 16.6 mg/L, 24.9 mg/L, 33 mg/L and 40 mg/L are 18.9±1.3 (relative standard deviation, *RSD*=6.2%), 33.6±2 (*RSD*=6.2%), 61.1±2.8 (*RSD*=6.3%), 79.3±3.7 (*RSD*=6.2%), 101.8±4.7 (*RSD*=6.3%) and 116.5±5.8 (*RSD*=6.3%), respectively. The improved sensitivity of this sensor

is due to the high surface-to-volume ratio of the dye entrapped core-shell silica nanoparticles, which also improves the accessibility of the dissolved oxygen to the dye molecules, and therefore enhances the quenching effect.

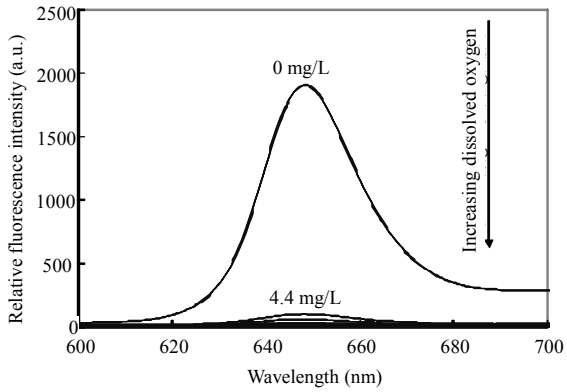

(a)

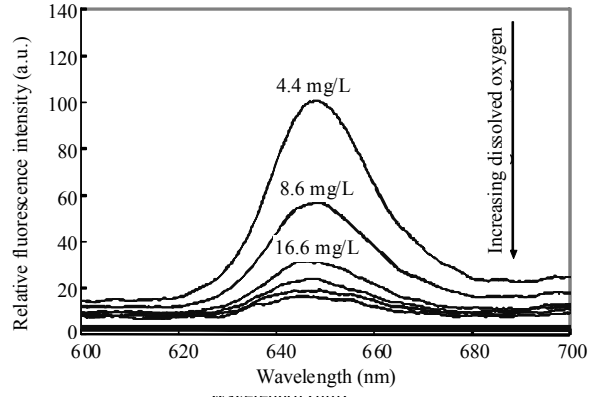

(b)

Fig. 7 Emission spectra of optical fiber sensor under different dissolved oxygen concentrations: (a) 0–40 mg/L and (b) 4.4 mg/L–40 mg/L [30].

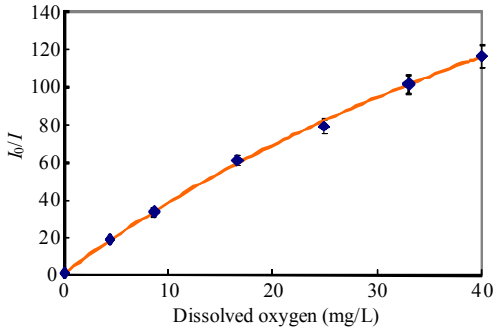

Fig. 8 Stern-Volmer plot of optical fiber dissolved oxygen sensor [30].

Table 3 compares the performance characteristics of the representative quenchometric dissolved oxygen sensors presented in the literature comprising Pt(II) or Ru(II) complexes embedded in various support matrices. Comparing the performance of various optical dissolved sensors, it is apparent that the sensor using Pt(II) complex and core-shell nanoparticles embedded in sol-gel matrix has a significantly higher sensitivity than those using Ru(II) complex dye. The PtTFPP-doped with dye entrapped core-shell silica nanoparticles dissolved oxygen sensor [30] has higher sensitivity (I_0/I_{100}~117) in the range of 0–40 mg/L.

Table 3 Comparison of performance characteristics of optical dissolved oxygen sensors.

Oxygen-sensitive dye	Support matrix	Response time	Sensitivity	Ref.
PtOEP	Fluorinated co-polymer matrix	Not available	I_0/I ~ 1.8 (0–40 mg/L)	[31]
$Ru(Ph_2phen)_3Cl_2$	Flurorpolymer matrix	Not available	I_0/I ~ 6.5 (0–30 mg/L)	[32]
$Ru(Ph_2phen)_3^{2+}$	TEOS/MTEOS	Not available	I_0/I ~ 3.5 (0–40 ppm)	[33]
$Ru(dpp)_3^{2+}$	TMOS/DiMe-DMOS	N_2 to O_2: 30 s O_2 to N_2: 100 s	I_0/I ~ 16 (0–100%)	[34]
$Ru(dpp)_3^{2+}$	TMOS/C_8TMOS	Not available	I_0/I ~ 10 (0–100%)	[35]
$Ru(bpy)_3Cl_2$	Silica-Ni-P Composite	N_2 to O_2: 200 s O_2 to N_2: 300 s	I_0/I ~ 2.5 (0–20×10^{-6} mM)(M,mol/L))	[36]
$Ru(dpp)_3Cl_2$	TMOS/DiMe-DMOS	N_2 to O_2: 66 s O_2 to N_2: 126 s	I_0/I ~ 7.3 (0–40 mg/L)	[37]
$Ru(dpp)_3^{2+}$	TEOS/MTEOS	Not available	I_0/I ~ 1.3 (0–45 mg/L)	[38]
PtTFPP and dye entrapped core-shell silica nanoparticles	TEOS/C_8TEOS	N_2 to O_2: 130 s O_2 to N_2: 694 s	I_0/I ~ 117 (0–40 mg/L)	[30]

$Ru(Ph_2phen)_3Cl_2$: Ru(II)-tris(4,7-diphenyl-1,10-phenanthroline) dichloride
$Ru(Ph_2phen)_3^{2+}$: Ru(II)-tris(4,7-diphenyl-1,10-phenanthroline)
$Ru(dpp)_3^{2+}$: Ru(II)-tris(4,7-diphenyl-1,10-phenanthroline) chloride
$Ru(bpy)_3Cl_2$: tris(2,2'-bipyridine)ruthenium dichloride
PtTFPP: platinum tetrakis pentrafluoropheny porphine
TEOS: tetraethoxysilane
TMOS: tetramethoxysilane
MTEOS: methyltriethoxysilane
DiMe-DMOS: dimethyldimethoxysilane
C_8TMOS: *n*-octyltrimethoxysilane
C_8TEOS: *n*-octyltriethoxysilane
I_0: the fluorescence intensities in the absence of oxygen
I: the fluorescence intensities in the presence of oxygen

2.2 Modified Stern-Volmer model for temperature compensation

Ideally, oxygen sensors should be temperature-independent such that they can be used in various environments. However, for optical sensors based on fluorescence quenching, both the fluorescence intensity and fluorescence decay time are influenced by ambient temperature. To account for the effects of temperature, many oxygen optrodes are designed to measure not only the oxygen concentration, but also the sensing temperature. With such sensors, an accurate indication of oxygen concentration is then obtained by applying a suitable temperature calibration factor to the measured oxygen concentration value.

In 2008, Lo *et al.* [39] developed a modified Stern-Volmer model to compensate for the temperature drift of oxygen concentration measurement obtained by fluorescent fiber-optic sensors. The basic concept of the proposed approach is to correct the Stern-Volmer constant to the reference Stern-Volmer constant at different temperatures. Therefore, the modified Stern-Volmer model has the form as

$$\frac{I_0(T_{\text{ref}})}{I_0(T_{\text{ref}})-I_{\text{m}}(T)}=\frac{1}{f_1(T)}\left(1+\frac{1}{K_{\text{sv1}}(T_{\text{ref}})[\%O_2(T)]}\right) \quad (4)$$

and

$$I_{\text{m}}(T)=I(T)C(T) \quad (5)$$

where $I_0(T_{\text{ref}})$ is the luminescence intensity in the absence of oxygen at the reference temperature (generally specified as room temperature), $I_{\text{m}}(T)$ is the modified luminescence intensity at the given temperature of the measurement environment, $I(T)$ is the steady-state luminescence intensity in the presence of O_2 at the given different temperatures of the measurement environment, $K_{\text{sv1}}(T_{\text{ref}})$ is the Stern-Volmer constant at the reference temperature, $f_1(T)$ is the fractional intensity of the component contributing to the total luminescence at the given temperature of the measurement, and $C(T)$ is the value of the temperature compensation coefficient at the given temperature of the measurement environment.

The temperature-compensated value of the oxygen concentration at any temperature T can then be derived from the measured fluorescence intensity $I(T)$ by applying the following rearranged form of (4) with the appropriate value of $C(T)$ and $f_1(T)$ taken from the calibration curve as

$$[\%O_2(T)]=\frac{I_0(T_{\text{ref}})-I(T)C(T)}{\left\{I_0(T_{\text{ref}})\left[f_1(T)-1\right]+I(T)C(T)\right\}K_{\text{sv}}(T_{\text{ref}})}. \quad (6)$$

Experimental results are fitted to the modified Stern-Volmer model in order to compute suitable values for a temperature compensation coefficient at different working temperatures. It is found that the proposed temperature compensation method can reduce the difference in the oxygen concentration measurement for working temperatures in the range of 25 ℃ to 70 ℃ as compared to data without compensation. The temperature-compensated measurement results obtained by two PtTFPP-doped oxygen sensors are plotted graphically in Figs. 9 and 10. The proposed approach could provide a straightforward and effective mean for improving the accuracy of fiber-optic oxygen sensors if a variable attenuator is designed according to temperature compensation coefficient. Thus, the fluorescent oxygen fiber-optic sensor with variable attenuator could work in a broad temperature range without temperature sensor.

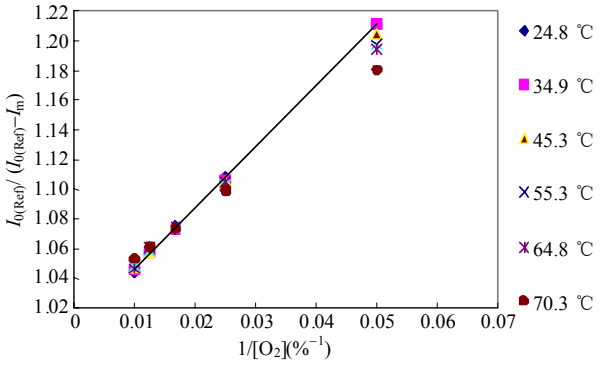

Fig. 9 Temperature-compensated oxygen concentration measurements obtained by PtTFPP-doped TEOS/Octyl-triEOS sensor [39].

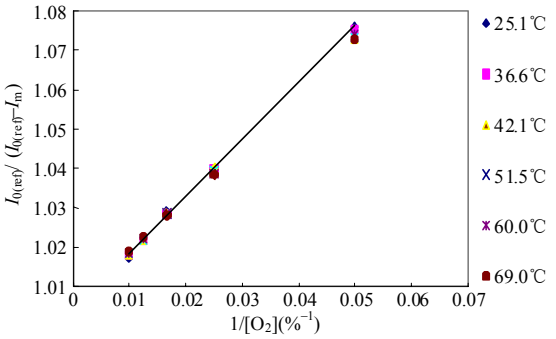

Fig. 10 Temperature-compensated oxygen concentration measurements obtained by PtTFPP-doped *n*-propyl-TriMOS/TFP-TriMOS sensor [39].

2.3 Simultaneous measurements on O_2 and temperature

In recent years, researchers have proposed various materials for dual sensing of temperature and oxygen. These sensing materials require the use of either a single wavelength or two different wavelengths for excitation purposes. Dual sensing techniques are commonly based on measuring the lifetime of the luminescence signal since this property is independent of drifts in the optical path, or variations in the gain of the detection system. Besides, the sensing layer embedded with multiple indicators occasionally displays the increased photodecomposition and signal drifts compared to single sensors, particularly when oxygen sensors (which generate singlet oxygen) are present [40]. Borisov and Wolfbeis [41] presented a fluorinated platinum porphyrin complex as an oxygen-sensitive probe, and a temperature-sensitive europium complex acting as a probe for temperature sensing. Two indicators yielded well-separated bright luminescence, and therefore two signals could be processed individually to provide independent values of oxygen and temperature, respectively. In 2008, Chu and Lo [42] presented a plastic optical fiber for dual sensing of temperature and oxygen, and the dimensions and sensing faces of the dual sensor are shown in Fig. 11. The sensor features commercially available epoxy glue coated on the side-polished fiber surface for temperature sensing and a fluorinated xerogel doped with PtTFPP coated on the fiber end for oxygen sensing. Dual sensing is performed using a single UV(ultraviolet) LED light source with the wavelength of 380 nm. The fluorescence emission spectra of two indicators are well resolved and exhibit no cross-talk effects.

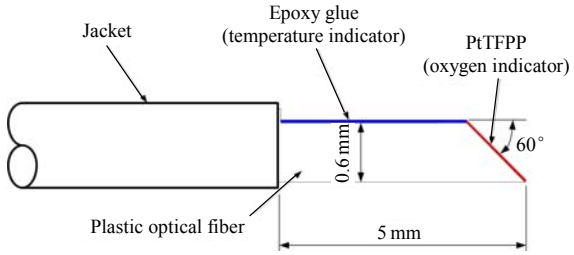

Fig. 11 Dimensions and sensing faces of plastic optical fiber sensor for dual sensing of temperature and oxygen [42].

Regression analysis can then be applied to determine the logarithmic relationship between luminescence intensity and temperature. Applying the equation $dB=10\times\lg(I_F^{22\,℃}/I_F)$ for temperature sensing, the data presented in Fig. 12(a) can be converted into the form of a linear calibration scale based on the attenuation of luminescence signal in dB, as shown in Fig. 12(b), where $I_F^{22\,℃}$ is the luminescence intensity of the sensor at 22 ℃ and I_F is the luminescence intensity at a measured temperature.

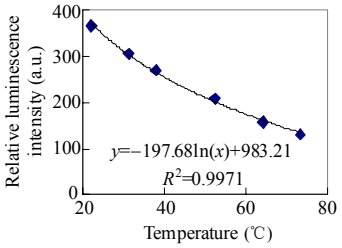

(a)

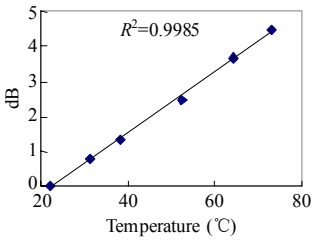

(b)

Fig. 12 Calibration curves of optical fiber dual sensor for temperature measurement: (a) calibration curve using luminescence intensity as sensing signal and (b) calibration curve using attenuation of luminescence signal in dB as sensing signal [42].

Figure 13 illustrates the Stern-Volmer plots of the optical fiber dual sensor derived from experimental data. It is observed that the plots corresponding to oxygen-sensing membrane are linear for temperature less than or equal to 38.1 ℃, which implies that the magnitude of luminescence quenching effect is directly related to oxygen concentration. In terms of temperature increasing from 52.4 ℃ to around 73.2 ℃, the Stern-Volmer plot becomes more and more nonlinear. The results of Fig. 13 confirm that the temperature response of epoxy glue membrane is insensitive to oxygen concentration. Thus, after the temperature is obtained by a dual sensor, a modified Stern-Volmer model introduced in Section 2.2 can be applied for measuring the oxygen concentration.

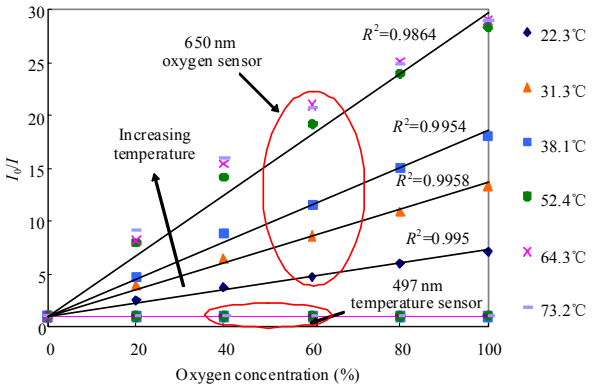

Fig. 13 Stern-Volmer plots of optical fiber dual sensor as function of oxygen concentration and temperature [42].

2.4 Full-field oxygen sensing

Two-dimensional (2D) measurement of the distribution of physical and chemical parameters in non-homogeneous samples is of interest in medical and biological researches. The combination of planar optodes and CCD technology leads to a significant improvement in the high spatial resolution two-dimensional mapping of single analytes in inhomogeneous samples. The best-known application of the long-life time fluorophores is for the oxygen imaging. Emission of many Ru(II) complexes and Pt(II) porphyrines is dynamically quenched by oxygen and can be effectively used as a lifetime oxygen sensors. Two-dimensional oxygen fluxes and partial pressure maps of surface oxygen have been monitored with such long-lived fluorophores as well as the time-domain and frequency-domain techniques [43–46].

In 2010, Chu and Lo [47] presented a modulation system for phase-resolved two-dimensional fluorescence phase imaging of a planar optical oxygen sensor. The proposed system is based on phase fluorometry technique and uses four-frame integrating-bucket method. Integrating buckets with multiple frames are achieved by using a complex programmable logic device to provide an external trigger to the CCD. The oxygen sensitive film is based on microporous film prepared by using a sol-gel process with a Pt(II) complex, PtTFPP, and the film can be efficiently excited by a laser diode with a central wavelength of 405 nm. Experimental results show that the maximum phase difference between 0 and 100% gaseous oxygen is 22°. The 2D full-field O_2 distribution imaging was found the most sensitive between 0 and 20% O_2. The combination of optical sensor technology and phase-resolved imaging allows the determination of the distribution of chemical or physical parameters in heterogeneous systems, which offers the proposed system a powerful testing tool for screening and mapping applications.

Figure 14 shows the 3D image extractions of phase shift at 0 oxygen concentration obtained by four-frame integrating-bucket method. The results confirm the feasibility of the proposed four-frame integrating-bucket method based on an external trigger mode of the CCD. The average phase shift of the optical oxygen sensor is 58.6° in a fully deoxygenated environment (i.e., 100% nitrogen) and 80.7° in a fully oxygenated environment. The maximum phase difference between 0 and 100% gaseous oxygen concentrations is thus 22° (Fig. 15). Furthermore, the results show a uniform phase shift distribution at low oxygen concentrations but a

non-uniform phase shift distribution at high oxygen concentrations. The non-uniformity of the phase shift distribution at high oxygen concentrations may be caused by the non-uniformity of the oxygen concentration distribution in the testing chamber.

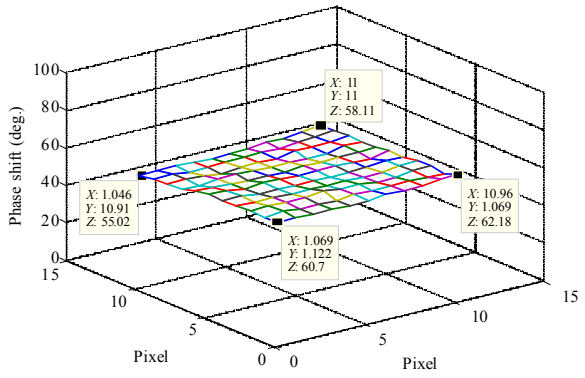

Fig. 14 Three dimensional image contours of the phase shift at 0 oxygen concentration by four-frame integrating-bucket method [47].

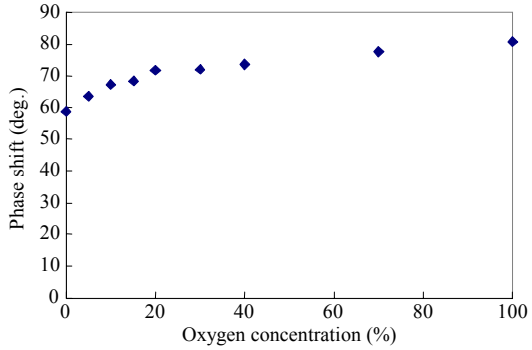

Fig. 15 Phase shift versus oxygen concentration for a sensor using four-frame integrating-bucket method [47].

3. Fluorescent carbon dioxide optical fiber sensors

Continuous and accurate sensing of carbon dioxide (CO_2) level in atmosphere is of fundamental importance in a wide variety of applications in chemical, clinical analysis and environmental monitoring fields. The CO_2 sensing techniques are mainly based on infrared (IR) absorptiometry [48], solid state electrochemical sensor device [49] and optical sensors [15]. Optical carbon dioxide sensors based on fluorescence intensity [15] or absorption changes [50] of pH indicators have several attractive features, including electrical isolation, reduced noise interference, possible miniaturization, and remote sensing. The pH-sensitive fluorescent dye 1-hydroxy-3,6,8-pyrenetrisulfonic acid trisodium salt has distinct absorption/emission bands in visible light region, and has been utilized in many aqueous-phase CO_2 optical sensors [10, 15, 13, 51–54]. In its protonated and deprotonated forms, the ion pair form of HPTS exhibits excitation peaks at wavelengths of 396 nm and 460 nm, respectively. The protonated form of HPTS emits in the blue region of the spectrum at a wavelength of 430 nm, whereas the deprotonated form emits in the green region at 515 nm. Specifically, the support material must have good solubility characteristics for the specific polar dye and should retain sufficient moisture to facilitate the water-mediated chemistry sensor.

The ORMOSIL matrix is characterized by transparency, photostability, and high sensitivity to the external environment. It is thus a potential solution to a variety of sensing applications. It has obvious advantages of chemical inertness and high porosity, which allow the encapsulation of analyte-sensitive dyes and enable fast transport of small molecules or ions through the sol-gel matrices. One disadvantage of ORMOSIL-based carbon dioxide sensors is their higher susceptibility to changes in humidity levels as compared to silicone or plasticised ethyl cellulose based sensors.

One of the sensing mechanisms for optical sensors for CO_2 relies on fluorescence intensity or quantum yield variation by interacting (quenching) with other chemical species. The most often used quenching mechanisms are resonance energy transfer (RET) [12] and inner-filter effects [55]. In the first case, the transfer of excited state energy takes place from a donor to an acceptor sensitive to CO_2 without the appearance of a photon, mainly as a result of dipole-dipole interactions between the donor and acceptor. In the case of inner-filter effects, the quenching is due to absorption of the excitation and/or emission radiation by the quencher.

In 2008, Chu and Lo [56] developed a CO_2 sensor based on pyranine pH-sensitive fluorescent indicator dye, tetraoctylammonium hydroxide (TOAOH) as the phase transfer agent (i.e. the base) and *n*-propyl-TriMOS/TFP-TriMOS as the support matrix. The use of hybrid xerogels is intended to improve both the sensitivity and the response time of the CO_2 sensor. The experimental results indicate that the fluorescence intensity of the HPTS dye decreases as the CO_2 gas phase concentration increases. The sensor has a sensitivity of approximately 18 (Fig. 16) and exhibits a linear response to CO_2 concentrations in the range of 0–30% (Fig. 17). The resolution is ±2.5% in this level and the limit of detection (LOD) is 0.03% CO_2, calculated as three times the standard deviation (3σ). The response time of the sensor is 1.7 s when being switched from a pure nitrogen atmosphere to a pure CO_2 atmosphere and 38.5 s from CO_2 to nitrogen.

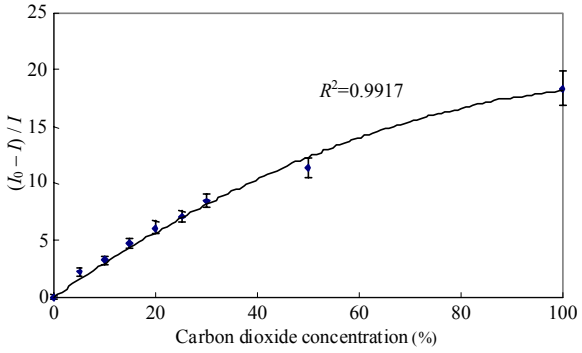

Fig. 16 Variation of $(I_0–I)/I$ with CO_2 concentration (0–100%) [56].

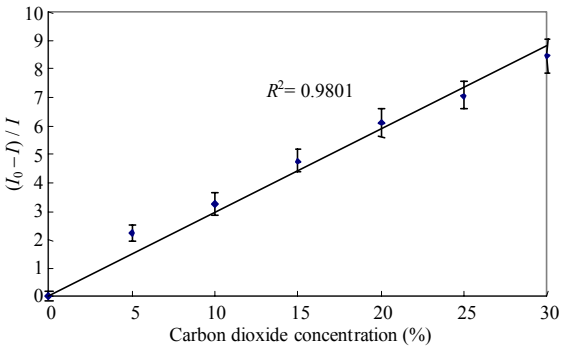

Fig. 17 Variation of $(I_0–I)/I$ with CO_2 concentration (0– 30%) [56].

In 2009, Chu and Lo [57] developed an optical fiber carbon dioxide sensor based on pH-sensitive fluorescent indicator dye, silica particles, tetraoctylammonium hydroxide (TOAOH) as the phase transfer agent (i.e. the base), and Octyl-triEOS/TEOS as the support matrix with uniquely enhanced sensitivity and linearity. The silica particles embedded in the sol-gel matrix were proposed to increase the surface area per unit mass of the sensing surface and it might play an important role in the increased sensitivity and linearity. The sensitivity and response time characteristics of the proposed device were evaluated by using a blue LED light source with a central wavelength of 460 nm and compared with those of various carbon dioxide sensors presented in the literature based on the ion pair form of HPTS immobilized in various sol-gel matrices. The sensor had a sensitivity of approximately 26 and exhibited a uniquely linear response to CO_2 concentrations in the range of 0–100% (Fig. 18).

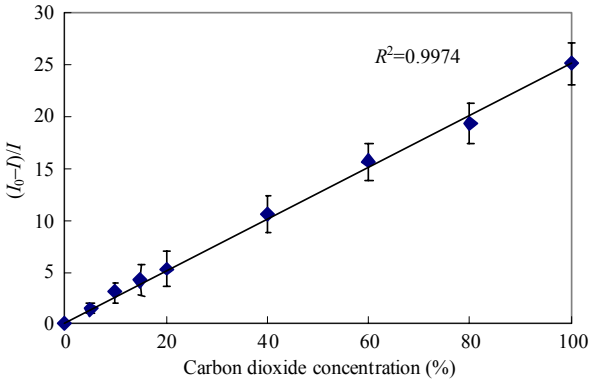

Fig. 18 Variation of $(I_0–I)/I$ with CO_2 concentration (0 –100%) [57].

Table 4 compares the performance of the representative CO_2 sensors fabricated by using the ion pair form of HPTS and various support matrices. The results show that the sensor based on Octyl-triEOS/TEOS sol-gel matrix doped with fluorescent dye ion pair form of HPTS and silica particles [53] has both higher sensitivity and better linearity than those of existing ion pair form of HPTS-based sensors; however, its response time is slower. The improved sensitivity of the current sensor can be attributed to the high

surface-to-volume ratio of silica particles, which improves the absorbance of carbon dioxide to the ion pair form of HPTS dye molecules.

Table 4 Comparison of response time and sensitivity characteristics of the representative CO_2 sensors fabricated with ion pair form of HPTS and various support matrices.

Sensitive dye	Matrix material	Storage conditions	Storage time	Dynamic working range	Sensitivity	Ref.
HPTS	Sol-gel matrix	Ambient conditions	Not available	0–20% CO_2	$I_{N_2}/I_{20\%CO_2}$ ~3	[15]
HPTS	Polymer matrix	Under different conditions	Under different storage times	2%–100% CO_2	$I_{N_2}/I_{100\%CO_2}$ ~7	[52]
HPTS	Ethyl cellulose matrix	Ambient conditions	2 months	0–10 hPa pCO_2	I_{0hPa}/I_{10hPa} ~2.3	[53]
HPTS	Ethyl cellulose matrix	Ambient conditions	Not available	0–20 hPa pCO_2	I_{0hPa}/I_{20hPa} ~2.6	[54]
HPTS	Sol-gel matrix	High humidity level	70 days	0–100%CO_2	$I_{N2}/I_{100\%CO_2}$	[13]
HPTS	Sol-gel matrix	Ambient conditions	4 months	0–100%CO_2	$I_{N_2}/I_{80\%CO_2}$ ~2	[10]
HPTS	Sol-gel matrix	None	Not available	0–100%CO_2	$I_{N_2}/I_{100\%CO_2}$ ~18	[56]
HPTS	Sol-gel matrix doped with silica particles	Sealed in the plastic bag with N_2 under humid condition	6 weeks	0–100%CO_2	$I_{N_2}/I_{100\%CO_2}$ ~26	[57]
HPTS	Cellulose matrix	Ambient conditions	95 days	1%–100%CO_2	$I_{N_2}/I_{100\%CO_2}$ ~3	[58]
HPTS	Polymer matrix	None	Not available	0–100%CO_2	$I_{N_2}/I_{100\%CO_2}$ ~ 6	[59]
HPTS	RTILs	Ambient conditions	212 days	0–100%CO_2	$I_{N_2}/I_{100\%CO_2}$ ~10	[60]

HPTS: 1-hydroxy-3,6,8-pyrenetrisulfonic acid trisodium salt

RTILs:1-methyl-3-butylimidazolium tetrafluoroborate (RTIL-I) and 1-methyl-3-butylimidazolium bromide (RTIL-II)

I_{N_2} : the fluorescence intensities in the absence carbon dioxide

$I_{20\%CO_2}$: the fluorescence intensities in the 20% CO_2

$I_{80\%CO_2}$: the fluorescence intensities in the 80% CO_2

$I_{100\%CO_2}$: the fluorescence intensities in the 100% CO_2

I_{0hPa}: the fluorescence intensities in the 0hPa pCO_2

I_{10hPa}: the fluorescence intensities in the 10hPa pCO_2

I_{20hPa}: the fluorescence intensities in the 20hPa pCO_2

4. Conclusions

In this review, we discussed the optical fiber oxygen and carbon dioxide sensors, the highly sensitive sensors based on dye entrapped core-shell particles, a modified Stern-Volmer model for temperature drift, an optical fiber dual sensor, and a full-field measurement method.

The highly sensitive optical fiber O_2 sensor and dissolved O_2 sensor are fabricated by coating one end of an optical fiber with a PtTFPP complex and dye entrapped core-shell particles embedded in a TEOS/Octyl-triEOS sol-gel matrix. Furthermore, the highly sensitive optical fiber carbon dioxide sensor is based on sol-gel matrix composed of alkyl and perfluoroalkyl ORMOSILs doped with pH-sensitive fluorescent dye and silica nanoparticles.

We also introduced a modified Stern-Volmer model to compensate for the temperature drift of oxygen concentration measurements obtained by using the optical fiber sensors. The experimental results are fitted to the modified Stern-Volmer model in order to compute suitable values for the temperature compensation coefficients at different working temperatures. On the other hand, a simple, low-cost plastic optical fiber sensor for the dual sensing of temperature and oxygen is introduced. The fluorescence emission spectra of two indicators are well resolved and exhibit no cross-talk effects.

A full-field system combined with CPLD (complex programmable logic device) and image processing algorithm is introduced to measure the full-field oxygen concentrations. The 2D full-field O_2 imaging system, based on a CCD camera and a laser diode light source, was shown to be applicable to the measurement of the phase shift between the excitation and emission. The results clearly demonstrate the superiority of phase-based imaging and indicate the reliability and versatility of the tool for biological research.

Acknowledgment

The authors gratefully acknowledge the financial

support provided to this study by the National Science Council of Taiwan under Grant No. NSC 96-2628-E-006-005-MY3.

References

[1] J. N. Demas, B. A. Degraff, and P. B. Coleman, "Oxygen sensors based on luminescence quenching," *Anal. Chem*., vol. 71, no. 23, pp. 793A–800A, 1999.

[2] K. Tsukada, S. Sakai, K. Hase, and H. Minamitani, "Development of catheter type optical oxygen sensor and applications to bioinstrumentation," *Biosens. Bioelectron*., vol. 18, no. 12, pp. 1439–1445, 2003.

[3] E. VanderDonckt, B. Camerman, R. Herne, and R. Vandeloise, "Fiber-optic oxygen sensor based on luminescence quenching of a Pt(II) complex embedded in polymer matrices," *Sens. Actuators B Chem.*, vol. 32, no. 3, pp. 121–127, 1996.

[4] P. Douglas and K. Eaton, "Response characteristics of thin film oxygen sensors, Pt and Pd octaethylporphyrins in polymer films," *Sens. Actuators B Chem*., vol. 82, no. 2–3 , pp. 200–208, 2002.

[5] C. McDonagh, B. D. MacCraith, and A. K. McEcoy, "Tailoring of sol-gel films for optical sensing of oxygen in gas and aqueous phase," *Anal. Chem.*, vol. 70, no. 1, pp. 45–50, 1998.

[6] Y. Tang, E. C. Tehan, Z. Tao, and F. V. "Bright, sol-gel-derived sensor materials that yield linear calibration plots, high sensitivity, and long-term stability," *Anal. Chem.*, vol. 75, no. 10, pp. 2407–2413, 2003.

[7] R. M. Bukowski, R. Ciriminna, M. Pagliaro, and F. V. Bright, "High-performance quenchometric oxygen sensors based on fluorinated xerogels doped with [Ru(dpp)(3)](2+)," *Anal. Chem*., vol. 77, no. 8, pp. 2670–2672, 2005.

[8] T. J. Manuccia and J. G. Eden, "Infrared optical measurement of blood gas concentrations and fiber optic catheter," U.S., Patent 4,509,522, 1985.

[9] B. H. Weigl and O. S. Wolfbeis, "Capillary optical sensors," *Anal. Chem.*, vol. 66, no. 20, pp. 3323–3327, 1994.

[10] D. A. Nivens, M. V. Schiza, and S. M. Angel, "Multilayer sol-gel membranes for optical sensing applications: single layer pH and dual layer CO_2 and NH_3 sensors," *Talanta*, vol. 58, no. 3, pp. 543–550, 2002.

[11] A. Mills and Q. Chang, "Fluorescence plastic thin-film sensor for carbon dioxide," *Analyst*, vol. 118, no. 7, pp. 839–843, 1993.

[12] C. von Bultzingslowen, A. K. McEvoy, C. McDonagh, and B. D. MacCraith, "Lifetime-based optical sensor for high-level pCO_2 detection employing fluorescence resonance energy transfer," *Anal. Chim. Acta*, vol. 480, no. 2, pp. 275–283, 2003.

[13] C. von Bultzingslowen, A. K. McEvoy, C. McDonagh, B. D. MacCraith, I. Kliment, C. Krause, and O. S. Wolfbeis, "Sol-gel based optical carbon dioxide sensor employing dual luminophore referencing for application in food packaging technology," *Analyst*, vol. 127, no. 11, pp. 1478–1483, 2002.

[14] X. He and G. A. Rechnitz, "Linear response function for fluorescence-based fiber-optic CO_2 sensors," *Anal. Chem*., vol. 67, no. 13, pp. 2264–2268, 1995.

[15] C. Malins and B. D. MacCraith, "Dye-doped organically modified silica glass for fluorescence based carbon dioxide gas detection," *Analyst*, vol. 123, no.11, pp. 2373–2376, 1998.

[16] T. S. Yeh, C. S. Chu, and Y. L. Lo, "Highly sensitive optical fiber oxygen sensor using Pt(II) complex embedded in sol-gel matrices," *Sens. Actuators B Chem*., vol. 119, no. 2, pp. 701–707, 2006.

[17] C. S. Chu and Y. L. Lo, "High-performance fiber-optic oxygen sensors based on fluorinated xerogels doped with Pt(II) complexes," *Sens. Actuators B Chem.*, vol. 124, no. 2, pp. 376–382, 2007.

[18] Y. Tang, E. C. Tehan, Z. Tao, and F. V. Bright, "Sol-gel-derived sensor materials that yield linear calibration plots, high sensitivity, and long-term stability," *Anal. Chem*., vol. 75, no. 10, pp. 2407–2413, 2003.

[19] K. Kalyanasundaram, "Photophysics, photochemistry and solar energy conversion with tris(bipyridyl) ruthenium(II) and its analogues," *Coord. Chem. Rev.*, vol. 46, no. 1–2, pp. 159–244, 1982.

[20] C. S. Chu and Y. L. Lo, "Ratiometric fiber-optic oxygen sensors based on sol-gel matrix doped with metalloporphyrin and 7-amino-4-trifluoromethyl coumarin," *Sens. Actuators B Chem*., vol. 134, no. 2, pp. 711–717, 2008.

[21] X. Y. Wang, C. Drew, S. H. Lee, K. J. Senecal, J. Kumar, and L. A. Sarnuelson, "Electrospun nanofibrous membranes for highly sensitive optical sensors," *Nano Lett*., vol. 2, no. 11, pp. 1273–1275, 2002.

[22] S. Santra, K. M. Wang, R. Tapec, and W. H. Tan, "Development of novel dye-doped silica nanoparticles for biomarker application," *J. Biomed. Opt.*, vol. 6, no. 2, pp. 160–166, 2001.

[23] C. Barbe, J. Bartlett, L. G. kong, K. Finnie, H. Q. Lin, M. Larkin, S. Calleja, A. Bush, and G. Calleja, "Silica particles: a novel drug-delivery system," *Adv. Mater*., vol. 16, no. 21, pp. 1959–1966, 2004.

[24] B. H. Han, I. Manners, and M. A. Winnik, "Oxygen sensors based on mesoporous silica particles on layer-by-layer self-assembled films," *Chem. Mater*., vol. 17, no. 12, pp. 3160–3171, 2005.

[25] C. S. Chu, Y. L. Lo, and T. W. Sung, "Enhanced oxygen sensing properties of Pt(II) complex and dye entrapped core-shell nanoparticles embedded in sol-gel matrix," *Talanta*, vol. 82, no. 3, pp. 1044–1051, 2005.

[26] Y. Amao, T. Miyashita, and I. Okura, "Platinum tetrakis (pentafluorophenyl) porphyrin immobilized in polytrifluoroethylmethacrylate film as a photostable optical oxygen detection material," *J. Fluor. Chem.*, vol. 107, no. 1, pp. 101–106, 2001.

[27] S. K. Lee and I. Okura, "Photostable optical oxygen sensing material: Platinum tetrakis (pentafluorophenyl) porphyrin immobilized in polystyrene," *Anal. Comm.*, vol. 34, no. 6, pp. 185–188, 1997.

[28] B. J. Basu, "Optical oxygen sensing based on luminescence quenching of platinum porphyrin dyes doped in ormosil coatings," *Sens. Actuators B Chem.*, vol. 123, no. 1, pp. 568–577, 2007.

[29] A. N. Watkins, B. R. Wenner, J. D. Jordan, W. Xu, J. N. Demas, and F. V. Bright, "Portable, low-cost, solid-state luminescence-based O_2 sensor," *Appl. Spectrosc.*, vol. 52, no. 5, pp. 750–754, 1998.

[30] C. S. Chu and Y. L. Lo, "Optical fiber dissolved oxygen sensor based on Pt(II) complex and core-shell silica nanoparticles incorporated with sol-gel matrix," *Sens. Actuators B Chem.*, vol. 151, no. 1, pp. 83–89, 2010.

[31] R. N. Gillanders, M. C. Tedford, P. J. Crilly, and R. T. Bailey, "Thin film dissolved oxygen sensor based on platinum octaethylporphyrin encapsulated in an elastic fluorinated polymer," *Anal. Chim. Acta*, vol. 502, no. 1, pp. 1–6, 2004.

[32] R. N. Gillander, M. C. Tedford, P. J. Crilly, and R. T. Bailey, "A composite thin film optical sensor for dissolved oxygen in contaminated aqueous environments," *Anal. Chim. Acta*, vol. 545, no. 2, pp. 189–195, 2005.

[33] A. K. McEvoy, C. M. McDonagh, and B. D. MacCraith, "Dissolved oxygen sensor based on fluorescence quenching of oxygen-sensitive ruthenium complexes immobilized in sol-gel-derived porous silica coatings," *Analyst*, vol. 121, no. 6, pp. 785–788, 1996.

[34] X. Chen, Z. M. Zhong, Y. Q. Jiang, X. R. Wang, and K. Y. Wong, "Characterization of ormosil film for dissolved oxygen-sensing," *Sens. Actuators B Chem*., vol. 124, no. 2, pp. 233–238, 2002.

[35] Z. Y. Tao, E. C. Tehan, Y. Tang, and F. V. Bright, "Stable sensors with tunable sensitivities based on class II xerogels," *Anal. Chem.*, vol. 78, no. 6, pp. 1939–1945, 2006.

[36] X. L. Xiong, D. Xiao, and M. M. F. Choi, "Dissolved oxygen sensor based on fluorescence quenching of oxygen sensitive ruthenium complex immobilized on silica-Ni-P composite coating," *Sens. Actuators B Chem*., vol. 117, no. 1, pp. 172–176, 2006.

[37] H. L. Pang, N. Y. Kwok, L. M. C. Chow, C. H. Yeung, K. Y. Wong, X. Chen, and X. R. Wang, "ORMOSIL oxygen sensors on polystyrene microplate for dissolved oxygen measurement," *Sens. Actuators B Chem*., vol. 123, no. 1, pp. 120–126, 2007.

[38] F. H. Chu, J. J. Yang, H. W. Cai, R. H. Qu, and Z. J. Fang, "Characterization of a dissolved oxygen sensor made of plastic optical fiber coated with ruthenium-incorporated solgel," *Appl. Optics*, vol. 48, no. 2, pp. 338–342, 2009.

[39] Y. L. Lo, C. S. Chu, J. P. Yur, and Y. C. Chang, "Temperature compensation of fluorescence intensity-based fiber-optic oxygen sensors using modified Stern-Volmer model," *Sens. Actuators B Chem*., vol. 131, no. 2, pp. 479–488, 2008.

[40] S. Nagl and O. S. Wolfbeis, "Optical multiple chemical sensing: status and current challenges," *Analyst*, vol. 132, no. 6, pp. 507–511, 2007.

[41] S. M. Borisov and O. S. Wolfbeis, "Temperature-sensitive europium(III) probes and their use for simultaneous luminescent sensing of temperature and oxygen," *Anal. Chem*., vol. 78, no. 14, pp. 5094–5010, 2006.

[42] C. S. Chu and Y. L. Lo, "A plastic optical fiber sensor for the dual sensing of temperature and oxygen," *IEEE Photon. Technol. Lett*., vol. 20, no. 1, pp. 63–65, 2008.

[43] P. Hartmann, W. Ziegler, G. Holst, and D. W. Lubbers, "Oxygen flux fluorescence lifetime imaging," *Sens. Actuators B Chem.*, vol. 38, no. 1, pp. 110–115, 1997.

[44] G. Holst and O. Kohls, "A modular luminescence lifetime imaging system for mapping oxygen distribution in biological samples," *Sens. Actuators B Chem.*, vol. 51, no. 1–3, pp. 163–170, 1998.

[45] G. Holst and B. Grumwald, "Luminescence lifetime imaging with transparent oxygen optodes," *Sens. Actuators B Chem*., vol. 74, no. 1, pp. 78–90, 2001.

[46] T. Vo-Dinh, *Biomedical Photonics Handbook.* Boca Raton: CRC Press, 2003.

[47] C. S. Chu and Y. L. Lo, "2D full-field measurement of oxygen concentration based on the phase fluorometry technique that uses the four-frame integrating bucket method," *Sens. Actuators B Chem.*, vol. 147, no. 1, pp. 310–315, 2010.

[48] T. J. Manuccia and J. G. Eden, "Infrared optical measurement of blood gas concentrations and fiber

optic catheter," U.S., Patent 4,509,522, 1985.
[49] Y. Shimizu and N. Yamashita, "Solid electrolyte CO_2 sensor using NASICON and perovskite-type oxide electrode," *Sens. Actuators B Chem.*, vol. 64, no. 1, pp. 102–106, 2004.
[50] Y. Amao and N. Nakamura, "An optical sensor with the combination of colorimetric change of α-naphtholphthalein and internal reference luminescent dye for CO_2 in water," *Sens. Actuators B Chem*., vol. 107, no. 2, pp. 861–865, 2005.
[51] B. H. Weigl and O. S. Wolfbeis, "New hydrophobic materials for optical carbon dioxide sensors based on ion-pairing," *Anal. Chim. Acta*, vol. 302, no. 2, pp. 249–254, 1995.
[52] O. S. Wolfbeis, B. Kovacs, K. Goswami, and S. M. Klainer, "Fiber-optic fluorescence carbon dioxide sensor for environmental monitoring," *Mikrochim. Acta*, vol. 129, no. 3, pp. 181–188, 1998.
[53] G. Neurauter, I. Klimant, and O. S. Wolfbeis, "Fiber-optic microsensor for high resolution pCO_2 sensing in marine environment," *Fresenius J. Anal. Chem*., vol. 366, no. 5, pp. 481–487, 2000.
[54] K. Ertekin, I. Klimant, G. Neurauter, and O. S. Wolfbeis, "Characterization of a reservoir-type capillary optical microsensor for pCO_2 measurements," *Talanta*, vol. 59, no. 2, pp. 261–267, 2003.
[55] Y. Amao and N. Nakamura, "Optical CO_2 sensor with the combination of colorimetric change of α-naphtholphthalein and internal reference fluorescent porphyrin," *Sens. Actuators B Chem.*, vol. 100, no. 3, pp. 347–351, 2004.
[56] C. S. Chu and Y. L. Lo, "Fiber-optic carbon dioxide sensor base on fluorinated xerogels doped with HPTS," *Sens. Actuators B Chem.*, vol. 129, no. 1, pp. 120–125, 2008.
[57] C. S. Chu and Y. L. Lo, "Highly sensitive and linear optical fiber carbon dioxide sensor based on sol gel matrix doped with silica particles and HPTS," *Sens. Actuators B Chem.*, vol. 143, no. 1, pp. 205–210, 2009.
[58] O. Oter, K. Ertekin, and S. Derinkuyu, "Ratiometric sensing of CO_2 in ionic liquid modified ethyl cellulose matrix," *Talanta*, vol. 76, no. 3, pp. 557–563, 2008.
[59] O. S. Wolfbeis and L. J. Weis, "Fiber-optic fluorosensor for oxygen and carbon dioxide," *Anal. Chem.*, vol. 60, no. 19, pp. 2028–2030, 1988.
[60] O. Oter, K. Ertekin, D. Topkaya, and S. Alp, "Emission-based optical carbon dioxide sensing with HPTS in green chemistry reagents: room-temperature ionic liquids," *Anal. Bioanal. Chem.*, vol. 386, no. 5, pp. 1225–1234, 2006.